IFIT1 is rapidly evolving and exhibits disparate antiviral activities across 11 mammalian orders

Matthew B. McDougal[1], Anthony M. De Maria[1], Ian N. Boys[1], Emi Nakahara[1], and John W. Schoggins[1]*

[1]Department of Microbiology, University of Texas Southwestern Medical Center, Dallas, TX, USA

*To whom correspondence may be addressed. **Email:** john.schoggins@utsouthwestern.edu

Abstract

Mammalian mRNAs possess an N7-methylguanosine (m7G) cap and 2′O methylation of the initiating nucleotide at their 5’ end, whereas certain viral RNAs lack these characteristic features. The human antiviral restriction factor IFIT1 recognizes and binds to specific viral RNAs that lack the 5’ features of host mRNAs, resulting in targeted suppression of viral RNA translation. This interaction imposes a significant host-driven evolutionary pressure on viruses, and many viruses have evolved mechanisms to evade the antiviral action of human IFIT1. However, less is known about the virus-driven pressures that may have shaped the antiviral activity of IFIT1 genes across mammals. Here, we take an evolution-guided approach to show that the IFIT1 gene is rapidly evolving in multiple mammalian clades, with positive selection acting upon several residues in distinct regions of the protein. In functional assays with 39 IFIT1s spanning diverse mammals, we demonstrate that IFIT1 exhibits a range of antiviral phenotypes, with many orthologs lacking antiviral activity against viruses that are strongly suppressed by other IFIT1s. We further show that IFIT1s from human and a bat, the black flying fox, inhibit Venezuelan equine encephalitis virus (VEEV) and strongly bind to Cap0 RNAs. Unexpectedly, chimpanzee IFIT1, which differs from human IFIT1 by only 8 amino acids, does not inhibit VEEV infection and exhibits minimal Cap0 RNA-binding. In mutagenesis studies, we determine that amino acids 364 and 366, the latter of which is undergoing positive selection, are sufficient to confer the differential anti-VEEV activity between human and chimpanzee IFIT1. These data suggest that virus-host genetic conflicts have influenced the antiviral specificity of IFIT1 across diverse mammalian orders.

Introduction

Interferon-induced protein with tetratricopeptide repeats 1 (IFIT1) is an interferon-stimulated gene (ISG) that is capable of distinguishing between self and non-self RNA. Mammalian mRNAs possess an N7-methylguanosine (m7G) cap and 2′O methylation of the initiating nucleotide at their 5' end. Many viral RNAs, however, lack these characteristic features. IFIT1 is able to recognize and bind viral RNAs that lack a m7G cap, including 5' triphosphate (5'-ppp-RNA) or viral RNAs that possess a m7G cap but lack 2′O methylation of the initiating nucleotide (Cap0 RNA) (1, 2). Crystal structures of human IFIT1 bound to both 5'-ppp-RNA and Cap0 RNA have helped uncover biochemical and structural determinants of IFIT1 antiviral activity, including residues that confer RNA-binding properties (3). IFIT1 binding to viral RNA subsequently inhibits infection by decreasing the amount of accessible RNA from the pool of replicating viral RNA (4) and by interacting with eIF proteins required for translation of viral proteins (5).

Viral restriction via IFIT1 binding to non-self RNAs imposes a host-driven evolutionary pressure for viruses to evade the antiviral function of IFIT1, as many viruses have evolved various mechanisms to elude IFIT1 binding and viral suppression (5). This includes viruses encoding their own capping and 2'O methyltransferase enzymes, using internal ribosome entry sites (IRES) to allow cap-independent translation of viral proteins, using host mRNA caps through cap-snatching, or hindering IFIT1 binding with RNA structures (5). For the alphavirus Venezuelan equine encephalitis virus (VEEV), which has a positive-sense, single-stranded RNA (+ssRNA) genome, a secondary RNA structure in the 5' UTR of the pathogenic Trinidad strain occludes IFIT1 binding to viral RNA, whereas the IFIT1-sensitive TC-83 strain has a point mutation that destabilizes this RNA structure. This allows IFIT1 to bind viral RNA and inhibit viral infection (1). VEEV TC83 can be inhibited by both human IFIT1 and mouse Ifit1B, suggesting

similar mechanisms have been at least partially evolutionarily conserved to restrict viral infection by IFIT proteins. However, as viruses have evolved mechanisms to evade IFIT1 antiviral activity, IFIT1 may also experience evolutionary pressure to overcome viral evasion. We know little about how such virus-imposed constraints may have influenced *IFIT1* evolution across mammals, broadly.

Pathogenic viruses can cause severe disease or death in mammals, imposing a major selective pressure on their mammalian hosts to evolve mechanisms that restrict viral infection. In turn, there is pressure on viruses to evade host defenses. These “molecular arms races” of host-pathogen co-evolution are evident as many genes involved in antiviral immunity exhibit signatures of positive selection or rapid evolution. Computational evolutionary analyses of antiviral ISGs have revealed specific domains and residues that are rapidly evolving (6-8). Identifying these signatures of positive selection has uncovered functional determinants of antiviral function in antiviral effectors such as MX1 and TRIM5α (9, 10). In addition to evolutionary pressure from host-pathogen molecular arms races, IFIT1 may have also been influenced by gene recombination occurring between *IFIT1* and the *IFIT1B* gene (11). *IFIT1* genes have undergone duplication, gene loss, and recombination with *IFIT1B* in mammals, resulting in genes that exhibit differential antiviral activity However, this was only assessed in a few species, and the extent of differential antiviral activity of IFIT1 across Mammalia remains unknown. Recently, in a screen for antiviral ISGs from bats, we found that IFIT1 from the black flying fox displays particularly strong suppression of VEEV (12).

Together, these studies led us to hypothesize that evolution may have resulted in “species-specific” antiviral ability of IFIT1 orthologs. While previous studies have provided considerable insight into the antiviral mechanism and structure of some mammalian IFIT1 proteins, a comprehensive study into the antiviral specificity of IFIT1 orthologs remains lacking.

Accordingly, we sought to use evolutionary and functional methods to interrogate differences in antiviral activity and biochemical properties of mammalian IFIT1.

Results

IFIT1 is rapidly evolving in mammals

Many antiviral effectors exhibit signatures of positive selection, as restriction factors and the viruses they suppress are often engaged in "molecular arms races (6, 7)." Therefore, we hypothesized IFIT1 may be rapidly evolving, as IFIT1 is a potent antiviral effector that many viruses have evolved mechanisms to evade (5). To test this, we used established computational methods to determine if the *IFIT1* gene is rapidly evolving across diverse clades of mammals. Using Phylogenetic Analysis using Maximum Likelihood (PAML) (13), we determined that *IFIT1* exhibits signatures of rapid evolution in all clades tested (primates, bats, carnivores, and ungulates) (Fig 1A). Rodents were not included in this analysis, as a genetic ortholog of IFIT1 has been lost in many rodent species (11). While all lineages showed signs of rapid evolution, carnivore IFIT1s exhibited the least significant likelihood of pervasive positive selection. However, all mammalian lineages were also determined to have at least 2 sites of statistically significant positive selection (Fig 1A). Detection of positive selection in certain domains or at specific sites of restriction factors has been utilized to uncover genetic determinants of antiviral function (6, 7). Therefore, we sought to potentially uncover other sites in IFIT1 that may be engaged in host-pathogen conflicts using complementary methods to PAML. We next used Fast Unconstrained Bayesian AppRoximation (FUBAR) (14), another approach that had been used to identify rapidly evolving sites of restriction factors. Using FUBAR analysis, we further identified at least one site predicted to be undergoing significant rapid evolution for all clades except carnivores (Fig 1B). Another complementary analysis, Mixed Effects Model of Evolution (MEME) (15), identified several sites of positive selection for all linages of tested mammals (Fig

1C). To our knowledge, these signatures of positive selection in *IFIT1* have not previously been reported and suggest that evolutionary pressure has acted on multiple regions of IFIT1.

Human IFIT1 residue 193 exhibits mutational resiliency

We next focused on three codons in primate IFIT1 – encoding V170, L193, and L366 in the human ortholog – that were determined by at least two models to be evolving under positive selection (Fig 1D). We examined the location of each in solved IFIT1 structures for potential importance in RNA-binding. None of these residues had previously been reported to be involved in IFIT1 RNA-binding or antiviral function (2, 3). While crystal structures of human IFIT1 bound to RNA indicate that residues V170 and L366 are not near the RNA-binding region, L193 is part of the TPR4 loop which has been reported to act as a lid over the 3' exit of the RNA-binding tunnel (3) (Fig 2A, 2B). The TPR4 loop, located between α-helices 9 and 10, also has been suggested to play a role in mediating contacts between subdomain II and subdomain III (Fig 2B) (3). Specifically, L193 in human IFIT1 protrudes into the exit of the RNA-binding tunnel and comes into close contact with RNA (Fig 2C) (3). In addition, L193 is in close proximity to R187, which is required for IFIT1 RNA binding and antiviral function (2). Therefore, we sought to test the importance of L193 in the antiviral function of IFIT1. Our general strategy was to use CRISPR-Cas9 gene editing to silence endogenous IFIT1 in human cells, and then reconstitute expression by ectopic expression of IFIT1 193 mutants. We performed site-directed mutagenesis to generate point mutations in a CRISPR-resistant human IFIT1 clone that correspond to every possible amino acid at residue 193. Huh7.5 cells that were CRISPR-targeted for endogenous IFIT1 were transduced with lentiviral pseudoparticles to express each of the 193 mutant IFIT1s or appropriate controls. Cells expressing the IFIT1 point mutants were then challenged with VEEV encoding a GFP reporter, and infection was quantified by flow cytometry (Fig 2D). We observed that most amino acid substitutions at residue 193 were

tolerated by human IFIT1 with respect to antiviral function. In addition, Western Blotting determined that all IFIT1 point mutants were expressed to appreciable levels (Fig 2D, Bottom). Indeed, all mutants at position 193, whether hydrophobic or positively charged, inhibited VEEV similarly to the wild-type (193L) IFIT1 (Fig 2D). Polar amino acids introduced at position 193 also retained antiviral function (Fig 2D). Severe loss of function in anti-VEEV activity of IFIT1 was only notable with glycine or proline (~50% loss of antiviral function) or with negatively charged residues (~75-100% loss of antiviral function) (Fig 2D). This experiment demonstrated the resiliency of IFIT1 antiviral function despite introduction of mutations in rapidly evolving site 193 within the TPR4 loop.

IFIT1 orthologs from diverse mammals demonstrate species-specific antiviral activity

To better understand the consequences of the evolutionary pressures on IFIT1, we sought to test the antiviral activity of diverse mammalian IFIT1 orthologs against RNA viruses. To accomplish this, we cloned IFIT1 protein-coding sequences from 38 species (including 2 predicted IFIT1 sequences from horse) of mammals into lentiviral expression vectors. The chosen orthologs ranged from 60% to over 98% identical to human IFIT1 in protein coding sequence and encompassed 11 taxonomic orders (Fig 3A, Fig 3B, Supp Table 1) within the superorders Euarchontoglires, Laurasiatheria, Afrotheria, and Xenartha, thus representing extensive diversity in both sequence and evolutionary distance relative to human IFIT1. All IFIT1 orthologs were also N-terminally HA-tagged to allow for detection by western blot. After generating lentivirus pseudoparticles, we transduced human Huh7.5 cells with these 39 IFIT1 orthologs or appropriate controls and challenged IFIT1-expressing cells with two different RNA viruses encoding a GFP reporter, VEEV and vesicular stomatitis virus (VSV) . These viruses were chosen because of reported suppression by human IFIT1 through distinct mechanisms. VSV is a rhabdovirus with a negative sense single-stranded RNA genome. IFIT1 inhibits VSV by

binding to viral RNA ending in a triphosphate (5'-ppp-N), sequestering viral RNA from the replicating RNA pool (2). VEEV (TC-83 strain) is an alphavirus with a positive-sense single-stranded RNA genome and is restricted by IFIT1 due to the binding and translation inhibition of viral Cap0 RNA (m7G-ppp-N). This viral RNA possesses the canonical m7G cap but lacks 2'O methylation of the initialing nucleotide of the viral 5' UTR, allowing recognition and binding by human IFIT1 (1, 16). IFIT1-expressing cells were challenged with an MOI of 1 for both VSV-GFP and VEEV-GFP, and infection was quantified by flow cytometry (Fig 3C). IFIT1 orthologs capable of potently restricting VSV or VEEV infection, defined by inhibition of 70% or greater relative to control cells, were considered hits in this screen. VEEV infection was potently suppressed by eleven IFIT1 orthologs (African savannah elephant, Chinese pangolin, sheep, white-tailed deer, black flying fox, dromedary camel, orca, Angola colobus, big brown bat, human, and large flying fox) (Fig 3C). Five IFIT1 orthologs (orca, cape elephant shrew, dolphin, European rabbit, and nine-banded armadillo) inhibited VSV infection by at least 70% compared to control cells (Fig 3D). We were surprised that hits for each virus spanned such diverse mammalian clades, and that there was little overlap in orthologs that inhibit VEEV and VSV. Also unexpected, many IFIT1 orthologs exhibited no antiviral activity against these two viruses, as only 10 of the 39 tested orthologs met our threshold to be considered hits. Western blotting determined that IFIT1 expression was not uniform during the ortholog screen (Supp Fig 1), suggesting that low expression of certain orthologs may have contributed to lack of antiviral function. Expression of certain IFIT1 orthologs (e.g. orca and European rabbit) was much higher than others, and some IFIT1 orthologs were expressed at very low levels (e.g. African green monkey and greater horseshoe bat) (Supp Fig 1). In addition, black-capped squirrel monkey IFIT1 was observed to run at a lower-than-expected molecular weight, suggesting a truncation or cleavage of the protein product (Supp Fig 1). However, it was noted that many IFIT1 orthologs were hits in the screens despite low expression, and only orca IFIT1 was a hit in both

VSV and VEEV screens despite very high expression by multiple orthologs. These data suggest that IFIT1 orthologs may exhibit species-specific antiviral functions independent of differences in protein expression.

Since expression of IFIT1 from distinct species was not equal during the ortholog screen, we sought to validate the antiviral phenotypes of a subset of orthologs with more comparable expression. We selected 9 orthologs for follow-up based on protein expression, evolutionary diversity, and variable phenotypes exhibited in the ortholog screen. Those chosen for validation and follow-up included IFIT1 from Chinese pangolin (hereafter referred to as pangolin), orca, sheep, black flying fox, big brown bat, chinchilla, human, chimpanzee, and cape elephant shrew (hereafter referred to as shrew) (Fig 4A). Human Huh7.5 cells were transduced with differing doses of lentivirus pseudoparticles to normalize IFIT1 expression between this subset of orthologs. After puromycin selection, western blot analysis revealed that the expression of IFIT1 orthologs was relatively uniform, except for the higher expression of orca IFIT1 and notably lower expression of pangolin IFIT1 (Fig 4B). IFIT1-expressing cells were then challenged with VEEV (Fig 4C) and VSV (Fig 4D) at an MOI of 2 to validate results from the original IFIT1 ortholog overexpression screen. VSV was potently inhibited by orca and shrew IFIT1, while no other tested orthologs significantly suppressed infection. Thus, VSV may evade suppression by many mammalian IFIT1s. VEEV was potently inhibited by pangolin, sheep, black flying fox, big brown bat, and human IFIT1, while orca IFIT1 modestly inhibited VEEV. Strikingly, VEEV was not significantly inhibited by chimpanzee IFIT1 but was largely suppressed by human IFIT1. This was of keen interest as human and chimpanzee IFIT1 differ in protein sequence by only 8 amino acids, and one of these (residue 366) was identified as rapidly evolving by both FUBAR and MEME (Fig 1D). Together, these validation experiments demonstrate that mammalian IFIT1 species-specific differences in viral suppression are largely independent of expression differences. This is exemplified by potent restriction of VEEV by

pangolin and big brown bat IFIT1 despite low expression (Fig 4B and 4C). Furthermore, high-expressing sheep IFIT1 only restricted VEEV infection, but not VSV, and orca IFIT1 only modestly reduced VEEV infection despite much higher expression than all other IFIT1s (Fig 4B-D).

We further tested the ability of this subset of 9 IFIT1 orthologs to inhibit human parainfluenza virus type 3 (PIV3) (Fig 4E). PIV3 is a paramyxovirus with a negative sense, single-stranded RNA (-ssRNA) genome that is not previously reported to be inhibited by IFIT1. However, PIV3 was chosen for follow-up because human IFIT1 is a dominant antiviral effector towards the related human parainfluenza virus type 5 (PIV5) acting through an unknown mechanism (17). PIV3 was significantly restricted by shrew, pangolin, chinchilla, black flying fox, and big brown bat IFIT1 (Fig 4E). This was notable as human IFIT1 exhibited no antiviral activity towards PIV3, whereas it is a key component of IFN-mediated restriction of the related PIV5 (17). Chinchilla IFIT1 also exhibited disparate activities, as it did not inhibit VEEV (Fig 4C) or VSV (Fig 4D), yet significantly protected cells from PIV3 infection (Fig 4E). We then tested cells expressing the 9 selected IFIT1 orthologs for the ability to suppress another alphavirus related to VEEV, Sindbis virus (SINV) (Fig 4E). SINV was largely resistant to most mammalian IFIT1s, consistent with previous human IFIT1 studies. However, SINV was potently suppressed by orca IFIT1, and modestly suppressed by pangolin, sheep, and chinchilla IFIT1 (Fig 4E), highlighting a pattern of suppression that was distinct across the 9 orthologs relative to the alphavirus VEEV. Together, these data demonstrate that IFIT1 orthologs exhibit broad antiviral phenotypes towards a panel of viruses with both +ssRNA and -ssRNA genomes, largely independent of differences in protein expression.

Human, black flying fox, and chimpanzee IFIT1 protein exhibit species-specific RNA binding

As previously highlighted, human and black flying fox IFIT1 significantly protected cells from VEEV infection compared to a control, while chimpanzee IFIT1 did not (Fig 4C). The black flying fox (*Pteropus alecto*), is a model megabat species that is a reservoir for zoonotic viruses (18-20) and expresses restriction factors with unique antiviral activities (12, 21). While human and black flying fox IFIT1 share only 69% identity, human and chimpanzee IFIT1 are over 98% identical (Fig 3B, Supp Table 1). Therefore, IFIT1 from these three species were of particular interest for functional studies. Accordingly, we sought to determine if this variability in restricting VEEV was due to differences in Cap0 RNA-binding ability of IFIT1 orthologs.

To perform *in vitro* RNA-binding assays, recombinant IFIT1 proteins were generated. We performed an electrophoretic mobility shift assay (EMSA) to investigate the RNA-binding properties of three mammalian IFIT1 orthologs. RNA probes matching the first 41 nucleotides of the VEEV 5' UTR were generated for EMSA by *in vitro* transcription. Probes were capped by the faustovirus capping enzyme (22) to generate 5' ends that resemble physiological Cap0 VEEV RNAs. After incubation of IFIT1 protein with Cap0 RNA probes, protein:RNA complexes were run on native gels, which were stained with a nucleic acid dye to visualize band shifts (Fig 5A). Quantification of band shift intensity and area under the curve analysis revealed that black flying fox IFIT1 exhibited the strongest RNA binding activity (Fig 5B, 5C). Human IFIT1 also bound VEEV RNA, but to a lesser extent than black flying fox IFIT1. Little binding was observed by chimpanzee IFIT1, as band shift intensity was barely above that of a human RNA-binding deficient control (human IFIT1-R187H) (2, 3) (Fig 5B, 5C). These biochemical data are consistent with viral phenotypes (Fig 4C), suggesting that species-specific antiviral activities of IFIT1s can be partly explained by RNA binding potential.

Mutagenesis of primate IFIT1 reveals genetic determinants of IFIT1 antiviral function

While human IFIT1 exhibited potent VEEV restriction and significant VEEV Cap0 RNA binding, chimpanzee IFIT1 lacked these properties. Chimpanzee and human IFIT1 differ by only 8 amino acids (Fig 6A), prompting us to examine which residues underlie the phenotypic differences. We performed site-directed mutagenesis to generate point mutations in both human and chimpanzee IFIT1 that correspond to the divergent residues between the two proteins (Fig 6A). As 3 of the 8 residues, 362, 364, and 366, are in close proximity (Fig 6A), we also generated a triple mutant IFIT1 that has these residues swapped between chimpanzee and human IFIT1 (hereafter referred to as the 362/4/6 triple mut). Notably, one of these three sites, L366 in humans and M366 in chimpanzee, was determined to be rapidly evolving in 2 of the tested computational models (Fig 1D).

We transduced Huh7.5 cells with lentiviruses expressing wild type (WT), single point mutant IFIT1s, or 362/4/6 triple mut IFIT1. After selection of transduced cells with puromycin, stable cells were challenged with VEEV-GFP at an MOI of 2 and infectivity was quantified by flow cytometry (Fig 6B). Western blotting demonstrated near uniform expression of all human and chimpanzee IFIT1 mutants (Fig 6B). Cells expressing wild-type chimpanzee IFIT1 were infected by VEEV at a rate of about 50%, similar to the approximately 60% infection rate observed in control cells. WT human IFIT1-expressing cells were infected at a rate of less than 10%, demonstrating significant VEEV suppression. Interestingly, the only point mutation in human IFIT1 that resulted in a significant loss of antiviral activity was L366M. Cells expressing human IFIT1 with the L366M point mutant were infected at a rate roughly 4-fold higher than cells expressing WT human IFIT1 (Fig 6B). Introduction of a Q364R mutation in human IFIT1 also resulted in a partial loss of antiviral function, although this was not statistically significant. Furthermore, the 362/4/6 triple mut introduced into human IFIT1 resulted in a near complete loss of anti-VEEV function of human IFIT1(Fig 6B). The reciprocal was true for chimpanzee IFIT1, which significantly gained antiviral function when the M366L mutation was introduced.

Cells expressing chimpanzee IFIT1 M366L were roughly half as likely to be infected as cells expressing the WT chimpanzee IFIT1 (Fig 6B). In addition, R364Q mutant chimpanzee IFIT1 resulted in a moderate increase in antiviral activity; however, this was not statistically significant compared to wild-type chimpanzee IFIT1. Furthermore, the 362/4/6 triple mut chimpanzee IFIT1 potently suppressed VEEV infection at a nearly identical level to that of WT human IFIT1. Together, we show that residues N362, Q364, and L366 in human IFIT1 are necessary for viral suppression of VEEV. In addition, the mutations of S362N, R364Q, and M366L in combination are sufficient for chimpanzee IFIT1 to gain potent antiviral function.

Amino acids 362, 364, and 366 are generally conserved across IFIT1 from 20 different primate species (Fig 6C). Specifically, residue 366 is typically a hydrophobic amino acid, with 5 out of the 20 primate sequences analyzed having either a valine or methionine, as seen in chimpanzee IFIT1, instead of a leucine, which is present in human IFIT1 (Fig 6C). This suggests that leucine at position 366 might be important for robust antiviral function in primate IFIT1, although further experiments are necessary to confirm this role. Additional support for the importance of L366 comes from our findings that the only primate IFIT1, besides those of chimpanzees and humans, which was expressed at appreciable levels during the screen was that of the Angola colobus. This IFIT1 variant also potently inhibited VEEV infection and notably contains a leucine at residue 366, similar to human IFIT1 (Fig 3C, Supp Fig 1). Glutamine is conserved at site 364 in all primate species aligned except chimpanzee which encodes an arginine (Q364R), introducing a positive charge. Point mutants of residue 364 in chimpanzee and human IFIT1 exhibited moderate alterations in anti-VEEV function, though not statistically significant, suggesting that this amino acid may have a minor role in antiviral restriction that synergizes with L366.

To test if residues 364 and 366 synergize to confer antiviral specificity between human and chimpanzee IFIT1, 364 and 366 double mutants (referred to as 364/6 double mut) were generated for both chimpanzee and human IFIT1. Huh7.5 cells expressing to express wild-type (WT), 364/6 double mut, or 362/4/6 triple mut IFIT1s of both chimpanzee and human IFIT1 were then challenged with VEEV-GFP at an MOI of 2 and infection was quantified by flow cytometry (Fig 6D). Western blotting demonstrated uniform expression of all human and chimpanzee IFIT1 mutants (Fig 6D). As in previous experiments, wild-type human IFIT1 strongly suppressed VEEV infection while wild-type chimpanzee IFIT1 did not (Fig 6D). However, the 364/6 double mut and 362/4/6 triple mut of human IFIT1 both had a near complete loss of antiviral capacity, resulting in cells being infected at a similar rate as cells expressing the wild-type chimpanzee IFIT1 (Fig 6D). These results suggest that residues 364 and 366, but not residue 362, in human IFIT1 are necessary to confer anti-VEEV function. In contrast, cells expressing the 364/6 double mutant or the 362/4/6 triple mutant of chimpanzee IFIT1 potently suppressed VEEV infection at rates similar to those observed in cells expressing wild-type human IFIT1. No difference in antiviral potency was observed between chimpanzee IFIT1 with the 364/6 double mut or 362/4/6 triple mut, suggesting again that residue 362 does not play a key role in the differential antiviral properties of human and chimpanzee IFIT1. Together, these data indicate that out of 8 amino acids that differ between human and chimpanzee IFIT1, sites 364 and 366, in combination, comprise the underlying differences in anti-VEEV function.

We next examined the location of amino acids 364 and 366 in the solved crystal structure of human IFIT1 bound to RNA and in the chimpanzee IFIT1 structure predicted by AlphaFold. Residues 364 and 366 are located within the α-helix 18 within TPR7 of IFIT1 (Fig 6A, 6E). They are not predicted to contact RNA and are not located in direct proximity of the RNA-binding pocket (Fig 6E, 6F), suggesting they may regulate IFIT1 function in an allosteric manner.

Discussion

Here, combining evolutionary and functional data, we conclude that mammalian IFIT1s are rapidly evolving viral restriction factors that exhibit species-specific antiviral activity. Furthermore, differences between the ability of human and chimpanzee IFIT1 to restrict VEEV led to the unexpected discovery that 2 residues in α-helices 18 within the TPR7 domain of IFIT1 may partially determine primate IFIT1 antiviral capacity. Swapping amino acids 364 and 366 of the IFIT1 protein sequence between human and chimpanzee IFIT1, in combination, resulted in reciprocal antiviral phenotypes (Fig 6B, 6D). The structures of human and chimp IFIT1 suggest that these amino acids are not directly involved in RNA binding. Thus, they may be involved in conformational changes of IFIT1 during RNA-binding or other allosteric effects, though additional studies are needed to test this.

Our data also support a hypothesis in which the breadth of IFIT1 antiviral phenotypes may be, at least partially, explained by differences in RNA-binding ability. VEEV infection was most potently suppressed by black flying fox IFIT1, significantly inhibited by human IFIT1, and unaffected by chimpanzee IFIT1 (Fig 4C). This trend was similarly observed in RNA binding assays with a sequence identical to that of the Cap0 VEEV 5' UTR by EMSA (Fig 5). Black flying fox IFIT1 exhibited the strongest binding of VEEV Cap0 RNA, pronounced binding was observed by human IFIT1, with minimal VEEV Cap0 RNA binding by chimpanzee IFIT1 (Fig 5). These data are consistent with previous studies showing that the ability of IFIT1 to bind viral RNA is required for its antiviral function (4, 23).

The differential antiviral activity between IFIT1B and IFIT1 across several mammals was previously demonstrated by Daugherty et al.(11). This study used phylogenetic approaches to show that gene birth, gene loss and gene conversion occurred throughout vertebrate *IFIT* genes, resulting in extensive genetic diversity (11). Furthermore, through viral

infection assays and a yeast growth assay, the authors suggest different RNA-binding properties and disparate antiviral functions between primate IFIT1s and mouse Ifit1b (11). Our studies significantly expand the diversity of mammalian IFIT1s interrogated for antiviral function. Notably, based on our studies, IFIT1s across *Mammalia* are not universally antiviral against VEEV and VSV. In fact, antiviral specificity of IFIT1 orthologs is possibly quite narrow and highly dependent on which virus is being evaluated.

We additionally provide new data to support a model in which mammalian IFIT1s spanning diverse orders are rapidly evolving, and that in primates, this is occurring at functionally relevant sites that are not directly implicated in RNA binding. Our computational studies also identified amino acid 193 as rapidly evolving and a mutational scanning determined that this residue is mutationally resilient. This was similarly observed for TRIM5α, in which most mutations within the v1 loop did not affect antiviral potency (24). In addition, alteration of charge within the v1 loop of TRIM5α played a significant role in determining the antiviral outcome of TRIM5α mutants (24). We similarly observed that introduction of negatively charged residues at position 193 within the TPR4 loop of human IFIT1 ablated antiviral activity (Fig 2D). Therefore, mutational resiliency within a rapidly evolving residue of primate IFIT1 suggests that alteration of a single amino acid within restriction factor IFIT1 may not result in major gain or loss antiviral function. This may maximize the potential for adaptation during evolutionary arms races with viruses. However, we cannot rule out the potential major role of mutations at position 193 in combination with other mutations in IFIT1. Together, our data suggest that positions 193 is rapidly evolving in primates and may accommodate many different amino acids while retaining antiviral function.

Our study does have several limitations, however. All IFIT1 ortholog screens were performed by expressing IFIT1 from distinct species in human cells, which may potentially affect

natural antiviral function. For example, that some IFIT1 orthologs may bind viral RNA, but not interface with human proteins to effectively suppress translation, resulting in no antiviral activity when expressed in human cells. Furthermore, our biochemical assays focus on IFIT1 binding to Cap0 RNA only. This is due to comparative studies that have demonstrated IFIT1 has the strongest affinity for Cap0 RNA when compared to other RNAs, such as ppp-RNA (3). This allowed us to use human IFIT1 as a positive control for Cap0 RNA-binding with a strong signal-to-noise for comparative RNA binding assays between IFIT1 orthologs that were successfully purified. However, it is possible that differences in ppp-RNA binding may underlie differences in the antiviral potency of IFIT1 towards viruses such as VSV and PIV3. This study also does not address the possibility that differential viral evasion of IFIT1 proteins contributes to species-specific antiviral activity. Furthermore, we have only provided genetic, but not structural evidence for underlying differences in chimpanzee and human IFIT1 RNA-binding and antiviral activity. By mutagenesis assays we demonstrate that 2 amino acid changes confer antiviral activity between chimpanzee and human IFIT1. Additional insight into the role of these residues might be gained from molecular dynamics simulations using the crystal structure of human IFIT1 bound to Cap0 RNA as a template. Comparisons with the 364/366 double mutant might determine whether these substitutions alter conformational dynamics in a manner that disfavors RNA binding.

Summarily, our findings underscore the notion that unbiased screening, investigations of restriction factors from non-model mammalian species, and evolutionary-guided approaches may uncover novel findings in host-pathogen interactions.

Materials and Methods

Cells and cell culture

Huh7.5 and 293T cells (from C. Rice, The Rockefeller University) were maintained in “complete” DMEM (Gibco) supplemented with 10% FBS (Gibco) and 1× non-essential amino acids (NEAA; Gibco). All derived stable cells expressing selectable markers were grown in complete DMEM containing puromycin (Gibco; Huh7.5: 4μg/mL). All cells were incubated at 37°C in 5% CO_2. All cell lines have been STR profiled and confirmed negative for mycoplasma contamination by PCR testing (Venor GeM mycoplasma detection kit, Sigma).

Viruses and viral infections

Venezuelan equine encephalitis virus (TC-83 strain) infectious clone was obtained from I.Frolov. VEEV-GFP stocks were generated as previously described (25). Briefly, infectious clone plasmid was linearized, and RNA was in vitro transcribed with the mMESSAGE mMACHINE™ SP6 Transcription Kit (Invitrogen) followed by RNA clean-up with the MEGAclear™ Transcription Clean-Up Kit (Invitrogen). BHK-21J cells (8 x 10^6 cells) were then electroporated with 5μg of in vitro transcribed RNA and plated. Media was changed 18 h after plating, and the remaining supernatant was collected 8 h post-media change. After centrifugation to remove cell debris, virus-containing supernatants were aliquoted and stored at -80°C. Sindbis virus (SINV-GFP, clone S300 from M. Heise) (26) was generated as previously described. Vesicular stomatitis virus (VSV-GFP) (from J. Rose) and human parainfluenza virus type 3 (PIV3-GFP) (JS strain, from Peter Collins) were propagated by passaging in BHK-21J cells and storing clarified supernatants as virus stocks at -80°C. All viral infections were performed in DMEM supplemented with 1% FBS and 1x non-essential amino acids at a total volume of 0.2mL in 24-well tissue culture plates. After a 1 h incubation period, 0.3mL of complete DMEM was added to all wells until harvest. For analysis of viral infection by flow cytometry, cells were dissociated from the plate with 150μL Accumax (Innovative Cell Technologies) and then fixed in paraformaldehyde at a final concentration of 1%. Cells were allowed to fix for at least 30 min at

4°C and subsequently centrifuged at 1500 x *g* for 5 min. Supernatant was removed from cell pellets and fixed cells were then resuspended in FACS buffer (PBS [Gibco] supplemented with 3% FBS). Flow cytometry was performed on the Stratedigm S1000EON benchtop flow cytometer, with analysis in FlowJo software.

Cloning and plasmids

IFIT1 coding sequences were obtained from the NCBI database. IFIT1 sequences were cloned into the Gateway expression vector pSCRPSY (27). IFIT1 orthologs were synthesized as gBlocks (IDT) with Gateway compatible DNA sequences and an N-terminal HA tag. Human and chimpanzee IFIT1 point mutants were generated using site-directed mutagenesis PCR. Human and chimpanzee IFIT1 362/4/6 triple mutants and 364/6 double mutants were generated by Gibson cloning of gBlocks (IDT). For protein purification, IFIT1 protein coding sequences that were codon-optimized for bacterial expression were cloned into a modified pET28a bacterial expression vector, containing an N-terminal 6X-His tag followed by the yeast Sumo (smt3).

Western Blotting

Cells were lysed with M-PER (Mammalian Protein Extraction Reagent, Thermo Scientific) containing 1x complete protease inhibitor cocktail (Roche) at 4°C for 5 min with intermittent rocking. Lysate was then stored at -80°C. For running SDS-PAGE, lysate was thawed on ice, and mixed to a final concentration of 1x SDS Loading Buffer (0.2 M Tris-Cl pH 6.8, 5% SDS, 25% Glycerol, 0.025% Bromophenol Blue, and 6.25% beta-mercaptoethanol). Samples were run on 12% TGX FastCast acrylamide gels (Bio-Rad) and transferred to nitrocellulose membranes using a TransBlot Turbo system (Bio-Rad). Membranes were blocked with 5% milk in 1x Tris Buffered Saline, with Tween-20 (TBS-T [20mM Tris, 150mM NaCl, 0.1% Tween-20]) for at least 45min. Subsequent incubation with primary antibody (at dilutions between 1:500 to 1:5000) diluted in 1% milk in TBS-T was performed overnight, rocking at 4°C. Primary

antibodies probing for GAPDH (Proteintech Cat# 10494-1-AP, RRID:AB_2263076), IFIT1 (Proteintech Cat# 23247-1-AP, RRID:AB_2811269) and HA-tagged IFIT1 (Biolegend Cat# 901502, RRID:AB_2565006) were used in this study. After incubation with primary antibodies, membranes were washed 3 times with TBS-T by rocking for 5 min. Secondary antibodies (Goat anti-Rabbit 800CW and Goat anti-Mouse 680RD [LI-COR] at 1:5000 dilutions) diluted in 1x TBS-T were incubated with membranes for at least 45 min. Membranes were then washed 3 times with TBS-T by rocking for 5 min. Proteins were visualized using the LI-COR Odyssey FC imaging system.

Lentivirus production and transduction

To generate lentivirus pseudoparticles, 350,000 293Ts were plated onto poly-lysine coated 6-well plates. Lentiviral packaging plasmids expressing VSV-g and Gag-pol were then mixed with SCRPSY plasmids at a ratio of 0.1µg:0.5 µg:2.5 µg, respectively. Plasmids were incubated for 20 min with a mix of XtremeGENE9 transfection reagent (Roche) and OptiMEM (Gibco). Transfection complexes were then added to 293T cells in 1mL of DMEM supplemented with 3% FBS dropwise. After 6 h of incubation, media was changed to 1.5 mL of DMEM supplemented with 3% FBS. Supernatants containing lentiviral pseudoparticles were harvested at 48 and 72 h post-transfection. Lentiviral pseudoparticles were then processed by adding 4µg/mL Polybrene (Sigma), 20mM HEPES, centrifuging at 1500rpm for 5min to remove cell debris, and storing at -80°C until transductions.

Lentivirus transductions were performed in 6-well plates after plating 350,000 cells (Huh7.5). Final volume of transductions was either 1mL or 1.5mL of lentivirus mixed with “pseudoparticle” DMEM (DMEM supplemented with 3% FBS, 4µg/mL Polybrene, and 20mM HEPES) After a 6 h incubation at 37°C, 2mL of complete DMEM was added to all transductions. Transduced cells

were split into selection media 48h post-transduction and passaged for a minimum of three passages in selection media.

Protein Purification and RNA Electrophoretic mobility shift assay

IFIT1 protein coding sequences that were codon-optimized for bacterial expression were cloned into a modified pET28a bacterial expression vector, containing an N-terminal 6X-His tag followed by the yeast Sumo (smt3). Plasmids were transformed into Rosetta DE3 cells. Transformants were grown in Terrific Broth (TB) with 50 mg/L Kanamycin and 34 mg/L of Chloramphenicol and Antifoam B at 37 °C. At the OD_{600} of 0.4, the temperature was lowered to 18 °C. Protein expression was induced at OD_{600}=3 by addition of IPTG to 0.4 mM final concentration. Cells were harvested after an overnight incubation by centrifugation (OD_{600}=~8.5) and lysed in the lysis buffer (50 mM Tris-HCl pH 8, 500 mM NaCl, 15 mM Imidazole, 1 mM PMSF, 4 mM β-ME) by sonication. Cell lysates were cleared by centrifugation at 35,000 x g for 30 minutes. The cleared lysate was applied onto a gravity column with pre-washed Ni-NTA resin. Resin was washed with 50 mM Tris-HCl pH 8, 1 M NaCl, 30 mM Imidazole, 4 mM β-ME. Proteins were eluted with 50 mM Tris-HCl pH 8, 300 mM NaCl, 300 mM Imidazole, 2 mM DTT. Proteins were treated with Ulp1 protease overnight to remove the Sumo tag and passed over a size-exclusion column (HiLoad 16/600 Superdex 200 pg), equilibrated with 50 mM Tris 8.0, 150 mM NaCl, 1 mM DTT. Peak fractions were pooled, concentrated by ultrafiltration, and stored at -80 °C until use.

Protein stock concentration of IFIT1 orthologs was determined by diluting protein 1:5 in 1x TBE and measuring A280. Extinction coefficient was determined by ProtParam tool (Expasy), and subsequently used to calculate and normalize protein concentrations between stocks.

Before loading, native gels (10% 19:1 Acrylamide: Bis-acrylamide, 25mM NaCl, 1x TBE, 0.0005% APS, 0.001% TEMED) were pre-run with 1x TBE in a cold room for at least 2.5 h. While gels were pre-running, binding reactions were set up at room temperature after thawing and keeping both RNA and protein stocks on ice. All dilutions of protein and RNA were in 1x reaction buffer (50nM TRIS pH 8.0, 100mM NaCl, 1mM EDTA, 0.01mg/mL Heparin sodium sulfate, 2.5% Glycerol). For binding reactions, 50nM of Cap0 RNA was mixed 1:1 with 0, 80, 160, 240, 320, and 400nM of purified IFIT1 protein in a final volume of 20μL and incubated at room temperature for 20 min.

18 μL of RNA:Protein complexes were then run on pre-run native gels for 2.5 h at 100V in 1x TBE in a cold room. Gels were then stained with 1x SYBR Gold stain (ThermoFisher Scientific) diluted in 1x TBE for 20 min rocking at room temperature and imaged on a ChemiDoc Imaging System (BioRad) with UV transillumination. Band intensity was subsequently analyzed using ImageLab software (BioRad).

In vitro transcription and 5' capping of RNA probes

Uncapped RNA probes were generated using the T7 RiboMAX™ Express Large Scale RNA Production System (Promega). Manufacturer instructions were modified for generating short RNA probes. Briefly, 10μM of DNA oligos corresponding to the T7φ2.5 promoter sequence and the complementary T7φ2.5 promoter sequence followed by the first 41nt of the VEEV TC-83 strain 5' UTR sequence. Oligos were boiled at 95°C for 2-3 min and then slow cooled to room temperature to allow annealing. 1 μM of the annealed DNA oligos served as the template per 20μL T7 transcription reaction. RNA was purified according to manufacturer instructions using phenol:chloroform nucleic acid extraction (Promega).

To generate Cap0 RNA, purified uncapped RNA probes were modified using the Faustovirus Capping Enzyme (FCE) (NEB) using modified manufacturer instructions. Briefly, 100μL

reactions were composed of 20μL of uncapped RNA purified after T7 transcription (described above), 0.2mM SAM, 1mM GTP, 7500U of FCE, 1x FCE reaction buffer, 80U RNasin® Plus Ribonuclease Inhibitor (Promega), and nuclease-free water up to 100μL. Reactions were incubated at 42°C for 4.5 h and then another 0.5 h at 50°C. Cap0 RNA was then purified using the same phenol:chloroform nucleic acid extraction as performed after the T7 transcription reaction (Promega). Cap0 RNA was determined to be at least 95% Cap0 RNA (m7GpppA) by targeted LC/MS after Nuclease P1 (NEB) digestion at 37°C for 30 min followed by inactivation of enzyme at 95°C for 2 min. LC/MS was performed by the UT Southwestern Preclinical Pharmacology Core Facility.

Computational Evolutionary Analysis

IFIT1 coding sequences for all analyses were obtained from the NCBI database. Alignment of multiple sequences was performed using MUSCLE and ClustalW implemented in MEGA X (28). Maximum-likelihood trees were constructed in MEGA X, with standard settings. Trimmed alignments were then generated (29), and when required, ALTER(30) was used to convert file formats. MEME (31) and FUBAR (14) were performed with HyPhy (32) using the Datamonkey web application (33). To perform PAML analysis, we used default settings with the F3x4 codon frequency table within CodeML. Likelihood ratio tests were performed to compare model 7 versus model 8 and model 8 versus model 8a to determine the presence of positive selection. Bayes empirical Bayes testing was performed to determine specific residues that are adaptively evolving. Species trees were generated using the TimeTree database (34). FigTree software was then used to make trees shown in figures. Alignments and determination of amino acid identity to human IFIT1 was performed using ClustalOmega (35). Graphics comparing human and chimpanzee IFIT1 structures were generated using ChimeraX (36).

Statistical analysis

All statistical analyses were performed in GraphPad Prism 9. All graphs represent the mean of n=3 independent biological replicates with error bars representing standard deviation. ns, $p > 0.05$, *, $p < 0.05$, **, $p < 0.01$, ***, $p < 0.001$, and **** $p < 0.0001$.

Acknowledgements

This work was funded in part by grants to J.W.S: NIH Grant AI158124, The Welch Foundation (I-2013-20220331), and the UT Southwestern High Impact / High Risk Grant. John W. Schoggins holds an Investigators in the Pathogenesis of Infectious Disease Award from the Burroughs Wellcome Fund. We acknowledge Chris huh for the Orcinus orca vector image, which was used without manipulation under Creative Commons license CC BY-SA 3.0 DEED (https://creativecommons.org/licenses/by-sa/3.0/).

A

Clade	N	p-value (M7vsM8)	p-value (M8vsM8a)	omega (dN/dS)	Positively selected sites (BEB p>0.95)
Primate	20	0.0006088	0.0002588	0.53606	193, 200
Bat	9	0.000001492	0.000003884	0.58854	193, 196, 367
Carnivore	21	0.008238	0.02007	0.40348	3, 296
Ungulate	21	8.58E-15	3.73E-15	0.88076	28, 44, 194, 195, 196, 197, 198, 203, 245, 284, 302, 319, 321, 325, 329, 339, 370, 372, 407, 411, 417, 474

B

Clade	N	Positively Selected Sites (>0.95 Probability)
Primate	20	30, 170, 193, 240, 366
Bat	9	193
Carnivore	20	N/A
Ungulate	20	196, 325, 417

C

Clade	N	Positively Selected Sites (<0.05 threshold)
Primate	20	2, 136, 170, 251, 266, 366, 414
Bat	9	80, 84, 92, 115, 127, 131, 153, 193, 230, 232, 298, 351, 352, 466
Carnivore	20	3, 7, 11, 63, 322
Ungulate	20	109, 129, 190, 200, 264, 265, 266, 284, 295, 302, 325, 329, 339, 406, 417, 472

D

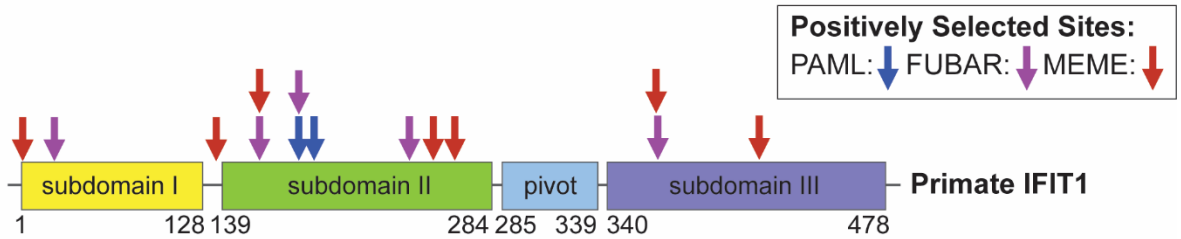

Figure 1. Evolutionary analysis of IFIT1 from clades of mammals reveals rapid evolution. A. PAML analysis was performed on coding sequences (procured from the NCBI database) that were trimmed aligned using CodeML. Likelihood ratio tests were performed to compare model 7 vs model 8 and model 8 vs model 8a to determine the presence of positive selection. N=number of sequences input, and numbers under “positively selected sites” represent residue number of the reference sequence. B. FUBAR analysis was performed on coding sequences (procured from the NCBI database) that were trimmed and aligned using HyPhy software and using the DataMonkey application. N=number of sequences input, and numbers under “positively selected sites” represent residue number of the reference sequence. C. MEME analysis was performed on coding sequences (procured from the NCBI database) that were trimmed and aligned using HyPhy software and the DataMonkey application. N=number of sequences input, and numbers under “sites of episodic positive selection” represent residue number of the reference sequence. D. Diagram of Primate IFIT1 domains and location of positively selected sites determined by PAML, FUBAR, and MEME.

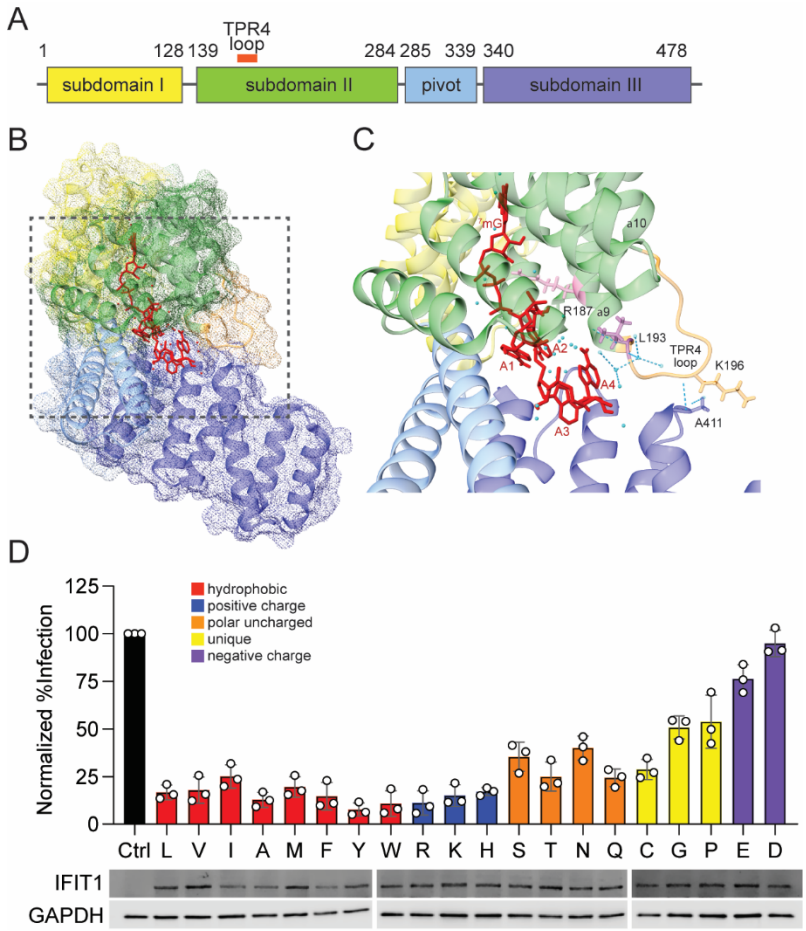

Figure 2. Mutagenesis of rapidly evolving residue 193 in human IFIT1 reveals mutational resiliency. A. Depiction of the human IFIT1 protein with the TPR4 loop location (red) shown. B. Solved crystal structure of IFIT1 bound to RNA with TPR4 loop forming a “lid” over the exit of the RNA-binding tunnel (PDB:5udj). C. Zoom in on the TPR4 loop and RNA-binding tunnel exit illustrating the location of the TPR4 loop and residue 193 in relation to bound RNA in the human IFIT1 crystal structure. D. Saturating mutagenesis screen of human IFIT1 with residue 193 mutated to every possible residue and challenged with VEEV infection. (Top) Huh7.5 that were CRISPR-targeted to silence endogenous IFIT1 were transduced with lentivirus to express IFIT1 mutants. Cells were then challenged with VEEV-GFP, and infectivity was quantified by flow cytometry. (Bottom) Western blot from lysates of Huh7.5 cells expressing IFIT1 point mutants.

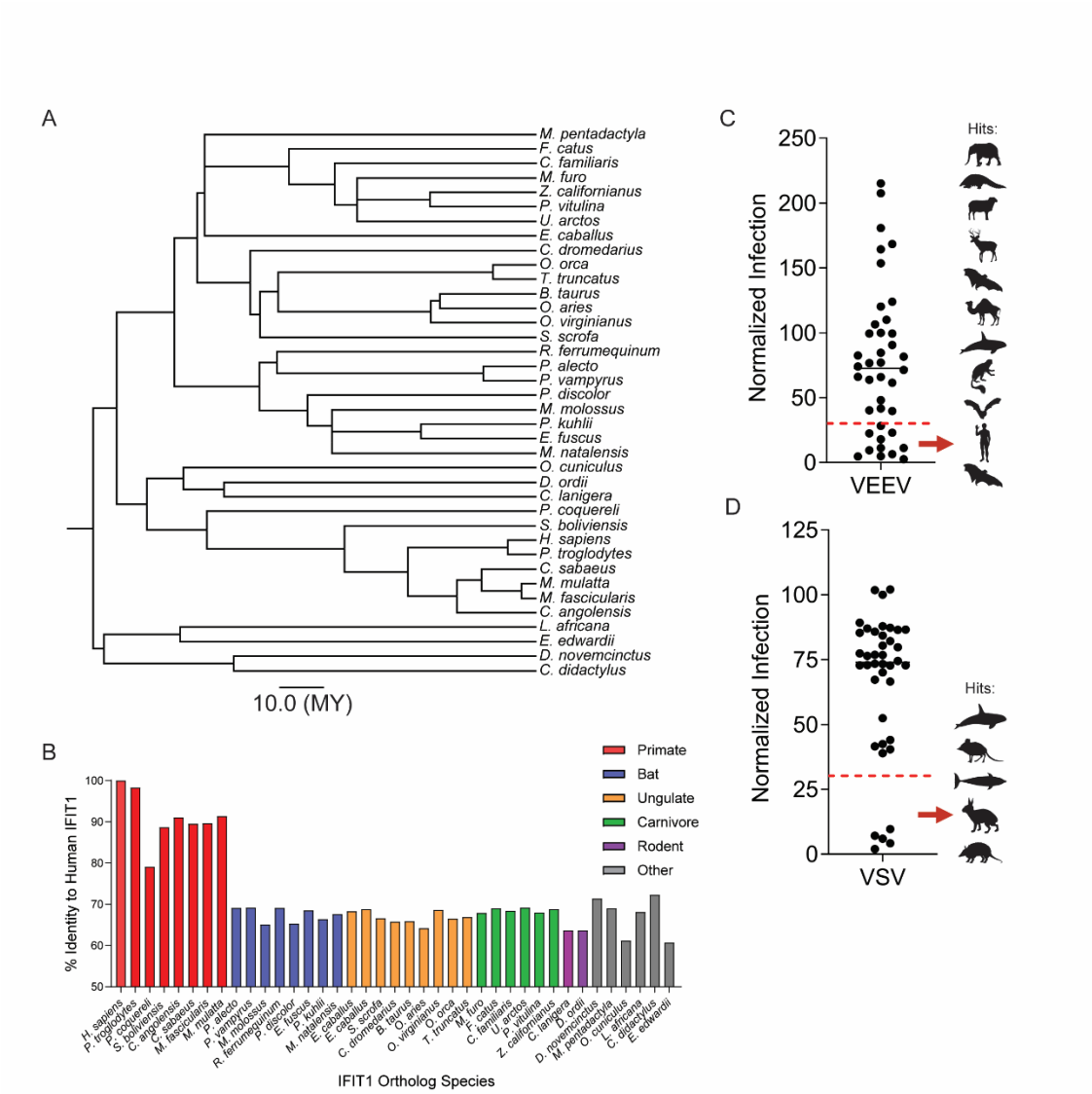

Figure 3. IFIT1 ortholog screens reveal extensive heterogeneity in mammalian IFIT1 antiviral function. A. TimeTree illustrating the evolutionary relationship of IFIT1 orthologs selected for ortholog screen. Scale bar represents divergence time of 10 million years. B. Graph illustrating protein sequence identity of IFIT1 orthologs used in screen relative to human IFIT1. C. Dot plot representing the relative infection (compared to control cells) from an ectopic overexpression screen in which Huh7.5 cells expressing 39 different IFIT1 mammalian orthologs were challenged with 1.0 MOI VEEV-GFP for 4 h. Infectivity was quantified by flow cytometry. Red line denotes 30% relative infection. Each data point represents the average of 2 biological replicates for VEEV-GFP. D. Same as C, for VSV-GFP (1 MOI, 4 h infection). Each data point represents the average of 3 biological replicates for VSV-GFP.

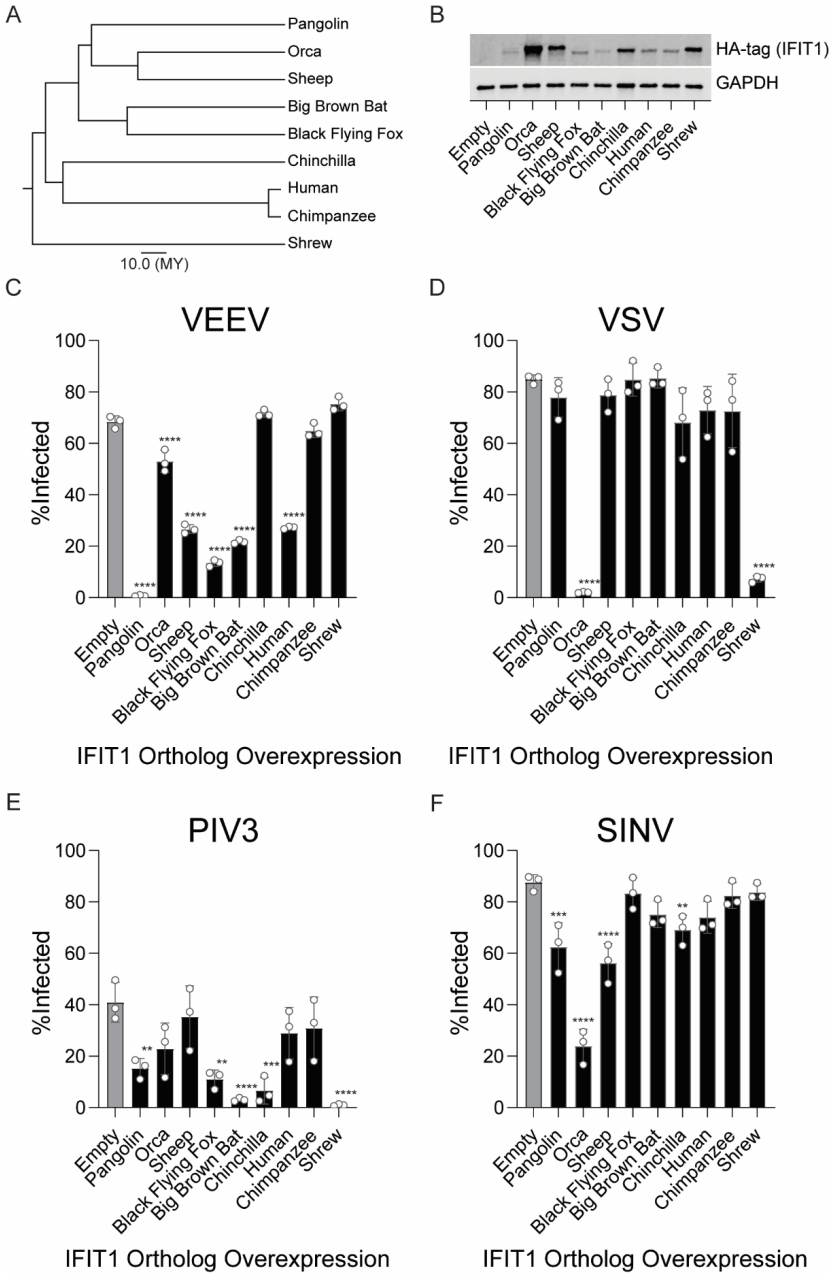

Figure 4. IFIT1 orthologs exhibit antiviral heterogeneity towards diverse RNA viruses. A. TimeTree illustrating the evolutionary relationship of IFIT1 orthologs selected for screen validation and follow-up. Scale bar represents divergence time of 10 million years. B. Western blot from cells expressing HA-tagged IFIT1 orthologs used in C-F. Image is representative of three independent replicates. C. Infection of IFIT1 ortholog-expressing Huh7.5 cells with VEEV-GFP (MOI 2, 4h) D. Infection of IFIT1 ortholog-expressing Huh7.5 cells with VSV-GFP (MOI 2, 4h) E. Infection of IFIT1 ortholog-expressing Huh7.5 cells with PIV3-GFP (MOI 2, 10h) F. Infection of IFIT1 ortholog-expressing Huh7.5 cells with SINV-GFP (MOI 2, 10h) . In C-F, data represent mean ± SD, n=3 biological replicates. Statistical significance determined by one-way ANOVA with Dunnett's test. ns $p > 0.05$, **$p < 0.01$, ***$p < 0.001$, and ****$p < 0.0001$.

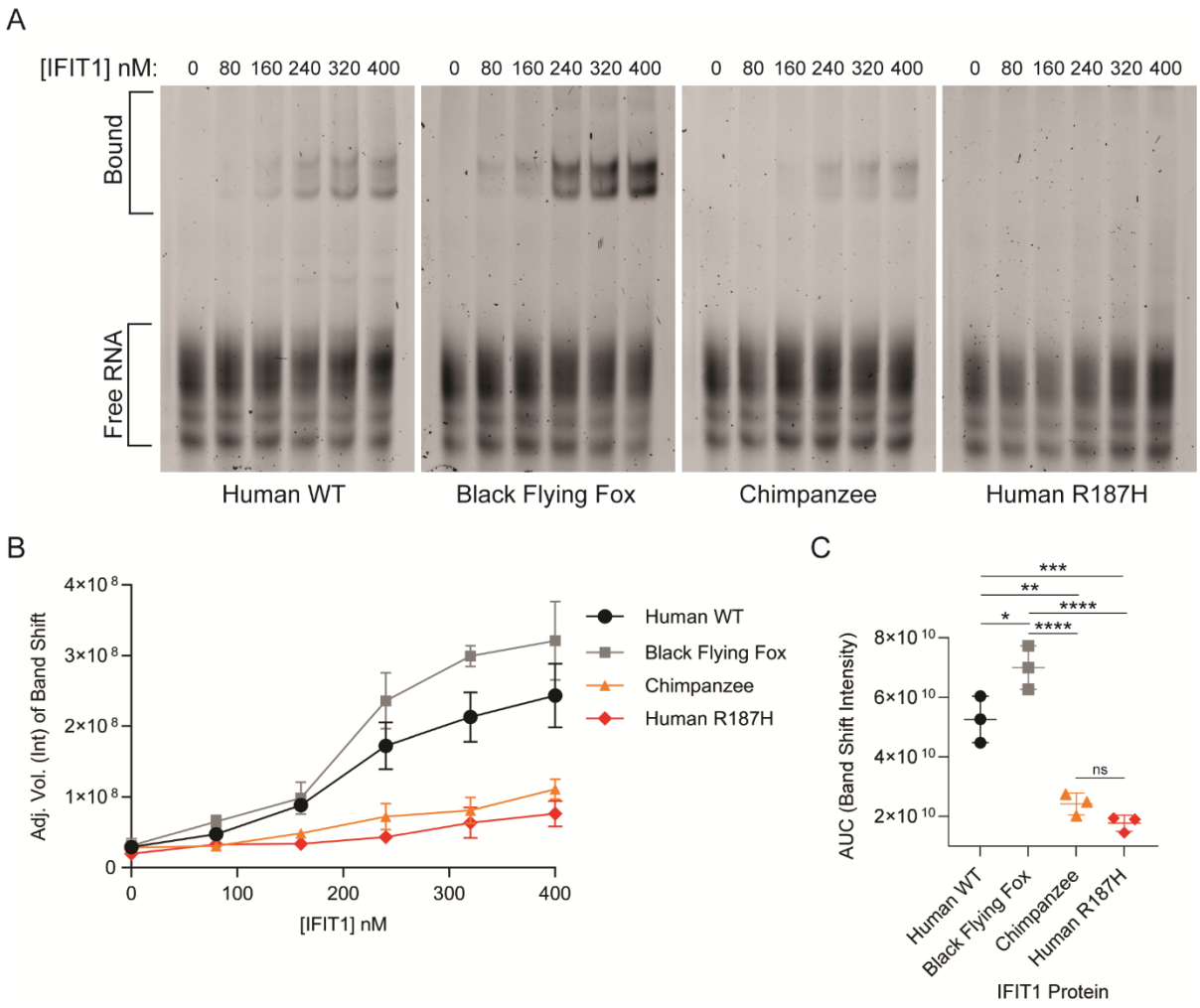

Figure 5. IFIT1 proteins exhibit species-specific Cap0 RNA binding. A. RNA EMSA with Cap0 VEEV RNA probes (41nt of VEEV TC-83 strain 5' UTR) at 50nM incubated with increasing concentrations of purified IFIT1 protein of mammalian orthologs and a negative control (human IFIT1-R187H). Images are one representative image from three independent replicates. B. Plot of the band shift intensity from EMSAs in A. Data represent mean ± SD, n=3. Band intensity was quantified by ImageLab software (BioRad). C. Area Under the Curve (AUC) analysis calculated from raw data in B. Statistical significance was tested by one-way ANOVA with correction for multiple comparisons. Data represent mean ± SD, n=3 replicates. ns, $p > 0.05$, *, $p < 0.05$, **, $p < 0.01$, ***, $p < 0.001$, and **** $p < 0.0001$.

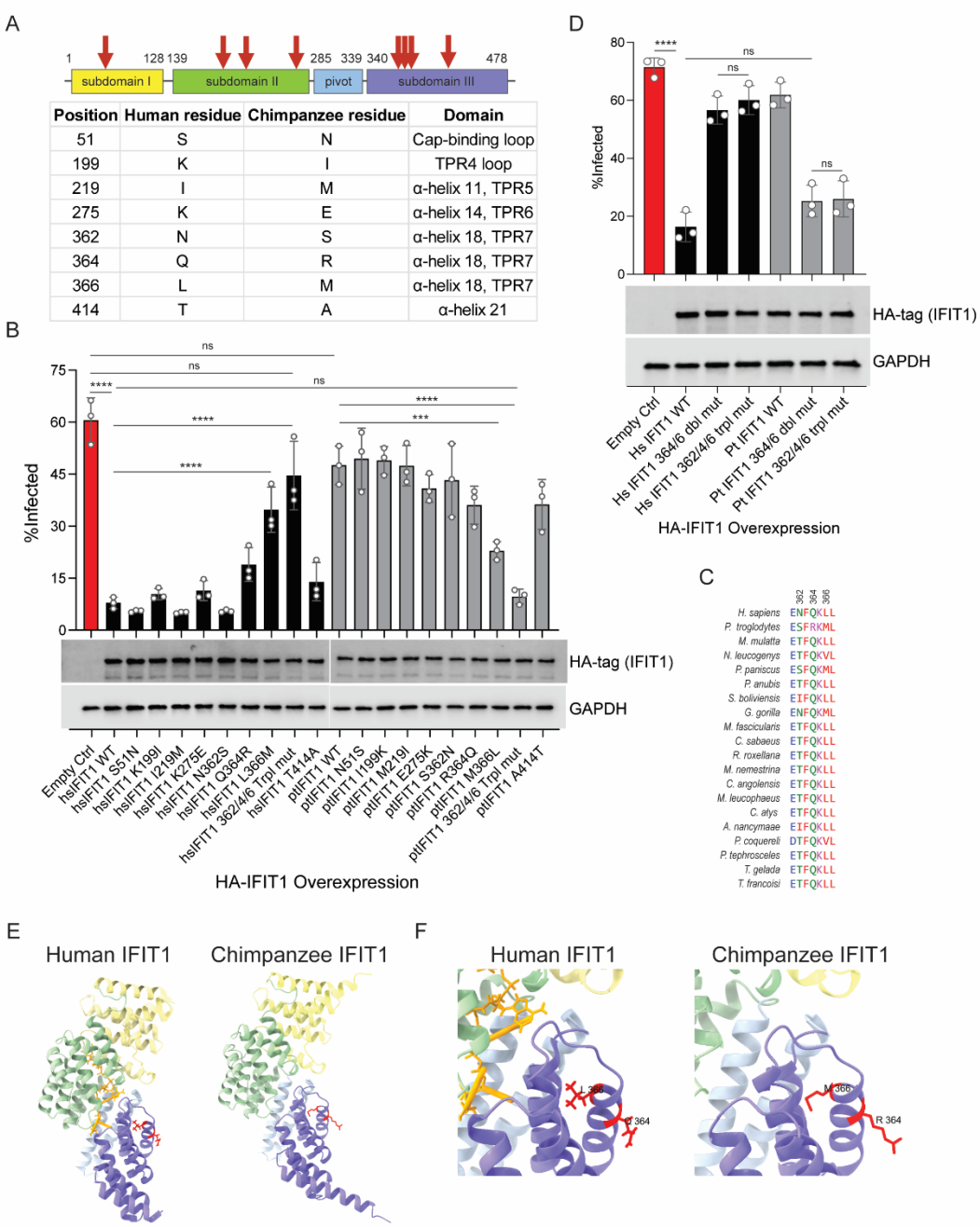

Figure 6. Mutagenesis uncovers genetic determinants of primate IFIT1 antiviral function. A. Diagram and chart describing amino acids that differ between human and chimpanzee IFIT1 as well as their domain location. B. Effects of primate IFIT1 mutant expression on VEEV-GFP infection. Huh7.5 cells were infected with an MOI of 2 for 4 h and infectivity was quantified by flow cytometry. Data represent mean ± SD, n=3 biological replicates. Statistical significance was determined by one-way ANOVA with Dunnett's test. ns, $p > 0.05$; ***, $p < 0.001$; and **** $p < 0.0001$. Western blotting for HA-tag (IFIT1) and GAPDH (Loading control) was also performed to determine expression levels of IFIT1 mutants. C. ClustalOmega protein sequence alignment of residues 361-367 of IFIT1 from 20 primate species. Sequences were obtained from the NCBI

database. D. Effects of primate IFIT1 double or triple mutant expression on VEEV-GFP infection. Huh7.5 cells were infected with an MOI of 2 for 4 h and infectivity was quantified by flow cytometry. Data represent mean ± SD, n=3 biological replicates. Statistical significance was determined by one-way ANOVA with Dunnett's test. ns, $p > 0.05$; and **** $p < 0.0001$. Western blotting for HA-tag (IFIT1) and GAPDH (Loading control) was also performed to determine expression levels of IFIT1 mutants. E. Structure of human IFIT1 bound to RNA (left) or AlphaFold predicted structure of chimpanzee IFIT1 (right) visualizing location of residues 364 and 366 (red) that confer antiviral activity. Graphics were generated using ChimeraX. F. Zoom in of (E).

A

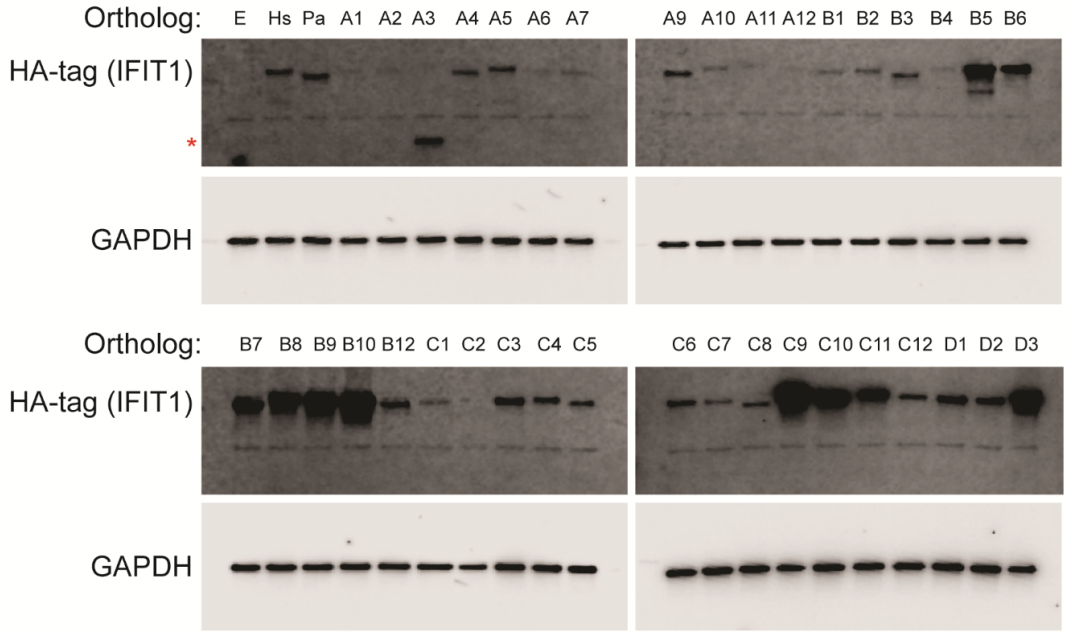

B

Common Name	Scientific Name	Key	Common Name	Scientific Name	Key
Empty Control	N/A	E	Cow	*Bos taurus*	B7
Human	*Homo sapiens*	Hs	Sheep	*Ovis aries*	B8
Black flying fox	*Pteropus alecto*	Pa	White-tailed deer	*Odocoileus virginianus texanus*	B9
African green monkey	*Chlorocebus sabaeus*	A1	Killer whale	*Orcinus orca*	B10
Coquerel's sifaka	*Propithecus coquereli*	A2	Common bottlenose dolphin	*Tursiops truncatus*	B12
Black-capped squirrel monkey	*Saimiri boliviensis*	A3	Ferret	*Mustela putorius furo*	C1
Angola colobus	*Colobus angolensis*	A4	Cat	*Felis catus*	C2
Chimpanzee	*Pan troglodytes*	A5	Dog	*Canis lupus familiaris*	C3
Crab-eating macaque	*Macaca fascicularis*	A6	Grizzly bear	*Ursus arctos horribilis*	C4
Rhesus macaque	*Macaca mulatta*	A7	Harbor (common) seal	*Phoca vitulina*	C5
Large flying fox	*Pteropus vampyrus*	A9	California sea lion	*Zalophus californianus*	C6
Velvety free tailed bat	*Molossus molossus*	A10	Nine-banded armadillo	*Dasypus novemcinctus*	C7
Greater horseshoe bat	*Rhinolophus ferrumequinum*	A11	Chinese pangolin	*Manis pentadactyla*	C8
Pale spear-nosed bat	*Phyllostomus discolor*	A12	European rabbit	*Oryctolagus cuniculus*	C9
Big brown bat	*Eptesicus fuscus*	B1	African savannah elephant	*Loxodonta africana*	C10
Kuhl's pipistrelle	*Pipistrellus kuhlii*	B2	Cape elephant shrew	*Elephantulus edwardii*	C11
Natal long-fingered bat	*Miniopterus natalensis*	B3	Linnaeus's two-toed sloth	*Choloepus didactylus*	C12
Horse 1	*Equus caballus*	B4	Ord's kangaroo rat	*Dipodomys ordii*	D1
Pig	*Sus scrofa*	B5	Chinchilla	*Chinchilla lanigera*	D2
Dromedary camel	*Camelus dromedarius*	B6	Horse 2	*Equus caballus*	D3

Supplementary Figure 1. IFIT1 ortholog expression varied during the ortholog screen. A. Western blot from lysates of cells expressing HA-tagged IFIT1 orthologs for screen in Fig 1A demonstrating unequal IFIT1 expression patterns. Images are representative of three independent replicates. B. Key denoting which symbols correspond to HA-tagged IFIT1 ortholog. Red asterisk marks the size of the truncated or cleaved protein product in lane A3.

References

1. Hyde JL, Gardner CL, Kimura T, White JP, Liu G, Trobaugh DW, et al. A viral RNA structural element alters host recognition of nonself RNA. Science. 2014;343(6172):783-7.
2. Pichlmair A, Lassnig C, Eberle CA, Gorna MW, Baumann CL, Burkard TR, et al. IFIT1 is an antiviral protein that recognizes 5'-triphosphate RNA. Nat Immunol. 2011;12(7):624-30.
3. Abbas YM, Laudenbach BT, Martinez-Montero S, Cencic R, Habjan M, Pichlmair A, et al. Structure of human IFIT1 with capped RNA reveals adaptable mRNA binding and mechanisms for sensing N1 and N2 ribose 2'-O methylations. Proc Natl Acad Sci U S A. 2017;114(11):E2106-E15.
4. Diamond MS, Farzan M. The broad-spectrum antiviral functions of IFIT and IFITM proteins. Nat Rev Immunol. 2013;13(1):46-57.
5. Hyde JL, Diamond MS. Innate immune restriction and antagonism of viral RNA lacking 2-O methylation. Virology. 2015;479-480:66-74.
6. Daugherty MD, Malik HS. Rules of engagement: molecular insights from host-virus arms races. Annu Rev Genet. 2012;46:677-700.
7. Duggal NK, Emerman M. Evolutionary conflicts between viruses and restriction factors shape immunity. Nat Rev Immunol. 2012;12(10):687-95.
8. Sironi M, Cagliani R, Forni D, Clerici M. Evolutionary insights into host-pathogen interactions from mammalian sequence data. Nat Rev Genet. 2015;16(4):224-36.
9. Mitchell PS, Patzina C, Emerman M, Haller O, Malik HS, Kochs G. Evolution-guided identification of antiviral specificity determinants in the broadly acting interferon-induced innate immunity factor MxA. Cell Host Microbe. 2012;12(4):598-604.
10. Sawyer SL, Wu LI, Emerman M, Malik HS. Positive selection of primate TRIM5alpha identifies a critical species-specific retroviral restriction domain. Proc Natl Acad Sci U S A. 2005;102(8):2832-7.
11. Daugherty MD, Schaller AM, Geballe AP, Malik HS. Evolution-guided functional analyses reveal diverse antiviral specificities encoded by IFIT1 genes in mammals. Elife. 2016;5.
12. Cruz-Rivera PCDL, Eitson JL, Schoggins JW. IRF7 from the black flying fox induces a STAT1-independent ISG response in unstimulated cell lines that protects against diverse RNA viruses. bioRxiv. 2024:2024.05.02.592239.
13. Yang Z. PAML 4: phylogenetic analysis by maximum likelihood. Mol Biol Evol. 2007;24(8):1586-91.
14. Murrell B, Moola S, Mabona A, Weighill T, Sheward D, Kosakovsky Pond SL, et al. FUBAR: a fast, unconstrained bayesian approximation for inferring selection. Mol Biol Evol. 2013;30(5):1196-205.
15. Murrell B, Wertheim JO, Moola S, Weighill T, Scheffler K, Kosakovsky Pond SL. Detecting individual sites subject to episodic diversifying selection. PLoS Genet. 2012;8(7):e1002764.
16. Reynaud JM, Kim DY, Atasheva S, Rasalouskaya A, White JP, Diamond MS, et al. IFIT1 Differentially Interferes with Translation and Replication of Alphavirus Genomes and Promotes Induction of Type I Interferon. PLoS Pathog. 2015;11(4):e1004863.
17. Andrejeva J, Norsted H, Habjan M, Thiel V, Goodbourn S, Randall RE. ISG56/IFIT1 is primarily responsible for interferon-induced changes to patterns of parainfluenza virus type 5 transcription and protein synthesis. J Gen Virol. 2013;94(Pt 1):59-68.
18. Halpin K, Young PL, Field HE, Mackenzie JS. Isolation of Hendra virus from pteropid bats: a natural reservoir of Hendra virus. J Gen Virol. 2000;81(Pt 8):1927-32.
19. Marsh GA, de Jong C, Barr JA, Tachedjian M, Smith C, Middleton D, et al. Cedar virus: a novel Henipavirus isolated from Australian bats. PLoS Pathog. 2012;8(8):e1002836.

20. Barr JA, Smith C, Marsh GA, Field H, Wang LF. Evidence of bat origin for Menangle virus, a zoonotic paramyxovirus first isolated from diseased pigs. J Gen Virol. 2012;93(Pt 12):2590-4.
21. Boys IN, Xu E, Mar KB, De La Cruz-Rivera PC, Eitson JL, Moon B, et al. RTP4 Is a Potent IFN-Inducible Anti-flavivirus Effector Engaged in a Host-Virus Arms Race in Bats and Other Mammals. Cell Host Microbe. 2020;28(5):712-23 e9.
22. Chan SH, Mole CN, Nye D, Mitchell L, Dai N, Buss J, et al. Biochemical characterization of mRNA capping enzyme from Faustovirus. RNA. 2023;29(11):1803-17.
23. Fensterl V, Sen GC. Interferon-induced Ifit proteins: their role in viral pathogenesis. J Virol. 2015;89(5):2462-8.
24. Tenthorey JL, Young C, Sodeinde A, Emerman M, Malik HS. Mutational resilience of antiviral restriction favors primate TRIM5alpha in host-virus evolutionary arms races. Elife. 2020;9.
25. Atasheva S, Krendelchtchikova V, Liopo A, Frolova E, Frolov I. Interplay of acute and persistent infections caused by Venezuelan equine encephalitis virus encoding mutated capsid protein. J Virol. 2010;84(19):10004-15.
26. Simmons JD, Wollish AC, Heise MT. A determinant of Sindbis virus neurovirulence enables efficient disruption of Jak/STAT signaling. J Virol. 2010;84(21):11429-39.
27. Kane M, Zang TM, Rihn SJ, Zhang F, Kueck T, Alim M, et al. Identification of Interferon-Stimulated Genes with Antiretroviral Activity. Cell Host Microbe. 2016;20(3):392-405.
28. Kumar S, Stecher G, Li M, Knyaz C, Tamura K. MEGA X: Molecular Evolutionary Genetics Analysis across Computing Platforms. Mol Biol Evol. 2018;35(6):1547-9.
29. Castresana J. Selection of conserved blocks from multiple alignments for their use in phylogenetic analysis. Mol Biol Evol. 2000;17(4):540-52.
30. Glez-Pena D, Gomez-Blanco D, Reboiro-Jato M, Fdez-Riverola F, Posada D. ALTER: program-oriented conversion of DNA and protein alignments. Nucleic Acids Res. 2010;38(Web Server issue):W14-8.
31. Murrell B, Weaver S, Smith MD, Wertheim JO, Murrell S, Aylward A, et al. Gene-wide identification of episodic selection. Mol Biol Evol. 2015;32(5):1365-71.
32. Kosakovsky Pond SL, Poon AFY, Velazquez R, Weaver S, Hepler NL, Murrell B, et al. HyPhy 2.5-A Customizable Platform for Evolutionary Hypothesis Testing Using Phylogenies. Mol Biol Evol. 2020;37(1):295-9.
33. Weaver S, Shank SD, Spielman SJ, Li M, Muse SV, Kosakovsky Pond SL. Datamonkey 2.0: A Modern Web Application for Characterizing Selective and Other Evolutionary Processes. Mol Biol Evol. 2018;35(3):773-7.
34. Kumar S, Stecher G, Suleski M, Hedges SB. TimeTree: A Resource for Timelines, Timetrees, and Divergence Times. Mol Biol Evol. 2017;34(7):1812-9.
35. Sievers F, Wilm A, Dineen D, Gibson TJ, Karplus K, Li W, et al. Fast, scalable generation of high-quality protein multiple sequence alignments using Clustal Omega. Mol Syst Biol. 2011;7:539.
36. Meng EC, Goddard TD, Pettersen EF, Couch GS, Pearson ZJ, Morris JH, et al. UCSF ChimeraX: Tools for structure building and analysis. Protein Sci. 2023;32(11):e4792.